OPUS-HSO

Repositorium der Hochschule Offenburg
https://opus.hs-offenburg.de

HOCH SCHULE OFFEN BURG

A grey-box model with neural ordinary differential equations for the slow voltage dynamics of lithium-ion batteries: Application to single-cell experiments

Jennifer Brucker, Rainer Gasper, Wolfgang G. Bessler

Zitiervorschlag im APA Stil:

Brucker, J., Gasper, R., & Bessler, W. G. (2024). A grey-box model with neural ordinary differential equations for the slow voltage dynamics of lithium-ion batteries: Application to single-cell experiments. *Journal of Power Sources*, *614*, 1–13. https://doi.org/10.1016/j.jpowsour.2024.234918

Abstract

Lithium-ion batteries exhibit a complex, nonlinear and dynamic voltage behaviour. Modelling their slow dynamics is a challenge due to the multiple potential causes involved. We present here a neural equivalent circuit model for lithium-ion batteries including slow voltage dynamics. The model uses an equivalent circuit with voltage source, series resistor, and diffusion element. The series resistance is parameterized using neural networks. The diffusion element is based on a discretized form of Fickian diffusion, parameterized using a neural network and learnable parameters. It is flexible to represent not only Warburg behaviour, but also resistor-capacitor-type dynamics. Mathematically, the resulting model is given by a differential–algebraic equation system combining ordinary and neural differential equations. Therefore, the model combines concepts of both physical theory (white-box model) and artificial intelligence (black-box model) to a combined framework (grey-box model). We apply this approach to a lithium iron phosphate based lithium-ion battery cell. The experimental voltage behaviour during constant-current cycles as well as the dynamics during pulse tests are well reproduced by the model. Only at very high and very low states of charge the simulation significantly deviates from experiments, which might result from insufficient training data in these regions.

Nutzungsbedingungen

Dieses Dokument wird unter diesen Bedingungen zur Verfügung gestellt:
Creative Commons - CC BY - Namensnennung 4.0 International
Für weitere Informationen siehe:
https://creativecommons.org/licenses/by/4.0/deed.de

Kontakt

Hochschule Offenburg | Bibliothek
Badstraße 24
77652 Offenburg
Telefon: (0781) 205-240
E-Mail: bibliothek@hs-offenburg.de
www.hs-offenburg.de/bibliothek

Journal of Power Sources 614 (2024) 234918

Contents lists available at ScienceDirect

Journal of Power Sources

journal homepage: www.elsevier.com/locate/jpowsour

A grey-box model with neural ordinary differential equations for the slow voltage dynamics of lithium-ion batteries: Application to single-cell experiments

Jennifer Brucker, Rainer Gasper *, Wolfgang G. Bessler

Institute of Sustainable Energy Systems (INES), Offenburg University of Applied Sciences, Badstraße 24, Offenburg, 77652, Baden-Württemberg, Germany

HIGHLIGHTS

- A new grey-box equivalent circuit model for lithium-ion batteries is developed.
- The model consists of a voltage source, series resistor, and diffusion element.
- Slow voltage dynamics is modelled with a grey-box diffusion model.
- The data-driven part of the grey box uses neural ordinary differential equations.
- The experimental voltage behaviour is well reproduced by the model.

ARTICLE INFO

Keywords:
Grey-box model
Equivalent circuit model
Lithium-ion battery
Diffusion
Neural ordinary differential equations

ABSTRACT

Lithium-ion batteries exhibit a complex, nonlinear and dynamic voltage behaviour. Modelling their slow dynamics is a challenge due to the multiple potential causes involved. We present here a neural equivalent circuit model for lithium-ion batteries including slow voltage dynamics. The model uses an equivalent circuit with voltage source, series resistor, and diffusion element. The series resistance is parameterized using neural networks. The diffusion element is based on a discretized form of Fickian diffusion, parameterized using a neural network and learnable parameters. It is flexible to represent not only Warburg behaviour, but also resistor-capacitor-type dynamics. Mathematically, the resulting model is given by a differential–algebraic equation system combining ordinary and neural differential equations. Therefore, the model combines concepts of both physical theory (white-box model) and artificial intelligence (black-box model) to a combined framework (grey-box model). We apply this approach to a lithium iron phosphate based lithium-ion battery cell. The experimental voltage behaviour during constant-current cycles as well as the dynamics during pulse tests are well reproduced by the model. Only at very high and very low states of charge the simulation significantly deviates from experiments, which might result from insufficient training data in these regions.

1. Introduction

Lithium-ion batteries are present in our everyday lives: they are a key technology for electric vehicles, portable devices and stationary applications such as home storage systems [1]. Upon dynamic operation (e.g., in electric vehicles), lithium-ion batteries exhibit a complex voltage and current behaviour on multiple time scales, ranging from milliseconds to hours [2]. The behaviour at long time scales (minutes and beyond) is not well understood today [3–6]. The present work focuses on these slow dynamics. It is an extension of our previous work on the topic [6].

Mathematical modelling and numerical simulation are excellent methods to understand and predict battery behaviour [7,8]. Different types of battery models are being used [6]. They can be generally categorized as white-box (WB), black-box (BB) and GB models. So-called WB models are based on thermodynamic, kinetic and transport theories. Therefore, they require a prior understanding of the underlying physics and chemistry. In contrast, so-called BB models approximate the relations between the system's input and its output based on empirical data only, without involving theories. They require a large amount of training data. Neural networks belong to the class of BB models [9,10]. So-called GB models combine WB and BB modelling

* Corresponding author.
E-mail addresses: jennifer.brucker@hs-offenburg.de (J. Brucker), rainer.gasper@hs-offenburg.de (R. Gasper), wolfgang.bessler@hs-offenburg.de (W.G. Bessler).

https://doi.org/10.1016/j.jpowsour.2024.234918
Received 14 February 2024; Received in revised form 6 June 2024; Accepted 15 June 2024
0378-7753/© 2024 The Author(s). Published by Elsevier B.V. This is an open access article under the CC BY license (http://creativecommons.org/licenses/by/4.0/).

techniques. GB models use prior theoretical knowledge and combine it with parametric parts. Unknown or imprecisely-known parameters and relationships are replaced by BB models. This leads to a reduced amount of required training data. GB models therefore combine the strengths of WB and BB methods [11–14].

ECMs are a common WB approach to simulate lithium-ion batteries [15–17]. Simple ECMs use one or more resistor-capacitor (RC) elements to describe the battery dynamics [2]. In some ECMs a ZARC element, the parallel connection of an ohmic resistor and a constant-phase element, is used [2]. An additional Warburg element can be used to account for the effects of Fickian diffusion of lithium within the electrodes [2,15,18–22]. While ECMs are formulated in a straightforward way in the frequency domain, their solution in the time domain is more challenging; this is true, in particular, for Warburg elements, which lead to a time-domain differential equation of fractional order [23]. Although only a small number of parameters are needed for ECMs, they show a strong and nonlinear dependence of operation conditions such as current and SOC. For these two reasons (difficult solution in the time domain and parameter dependence on operating conditions), we have introduced previously a GB circuit element for the slow voltage dynamics caused by transport processes, termed diffusion voltage, using neural ordinary differential equations (NODEs) [6]. The circuit element was based on the Fickian diffusion law, where the transport domain was discretized using finite volumes. Within the physical structure, unknown parameters (diffusion coefficient, diffusion length, discretization) and dependencies (SOC or lithium concentration) were replaced by neural networks and learnable parameters. As shown in Ref. [6], this approach can capture not only Warburg-type dynamic behaviour, but also RC circuit dynamics. In the present work, we apply this GB element into a battery ECM.

Several other previous works have introduced BB model elements into ECMs, which is briefly reviewed in the following. Wang et al. [24] used an ECM with an open-circuit voltage (OCV) source, a series ohmic resistor and one RC circuit to model a lithium-ion battery. The series ohmic resistance, the polarization resistance and capacitance as well as its dependencies on SOC and temperature were represented by a neural network. Luzi et al. [25] introduced a neural networks ensemble approach for modelling lithium-ion batteries. They used three neural networks to approximate the dynamic, the instantaneous, and the quasi-stationary voltage contributions. In a follow-up work, Luzi et al. [26] used a neural network to represent the OCV, and additional feedforward networks to approximate the ohmic resistances and the time constants of the RC circuits. Leonori et al. [27] combined the approaches of Refs. [25,26] to build a physically-inspired equivalent neural network circuit model. They replaced the OCV prediction with a more complex approach inspired by the fractional order formulation of an extended single particle model [28–30]. Li et al. [31] have simplified the extended single particle model through a fractional order approximation on the solid phase diffusion contribution. Neural networks were used to model the time constant and the ohmic resistance of the SOC dynamics. In our previous work [32] we have presented a GB model with NODEs. Our ECM consisted of an SOC-dependent voltage source, a hysteresis voltage drop, a constant series ohmic resistor and an RC circuit representing the charge transfer. The dependence of the charge-transfer resistance on battery current and SOC was captured by two neural networks, one for charging and one for discharging. This brief discussion of the literature makes it clear that there are quite different approaches towards integrating BB or GB features such as neural networks into ECMs.

In the present article, we introduce a novel Grey-Box ECM for lithium-ion batteries with a focus on long-timescale battery voltage dynamics. Fig. 1(a) shows an overview of the methodology. Starting from a simple WB ECM, a BB model ("BB" in Fig. 1(a)) is used to represent a series ohmic resistance. We add a GB model for slow voltage dynamics from Ref. [6] ("GB I" and "GB II" in Fig. 1(a)). The resulting Grey-Box ECM can describe the macroscopic voltage behaviour of a lithium-ion battery cell on multiple time scales (hours for charge or discharge, minutes for transport processes). It is normalized and the parameters are initialized based on estimates of the individual learnable parameters. The scaled model is then trained on the experimental data. Finally, the model is tested on data not included in the training process. For training and testing, we used the same experimental data considered previously [32], in particular, charge, discharge, pulse and dynamic cycle tests of a large-format 180 A h prismatic commercial lithium-ion cell with lithium iron phosphate (LFP)/graphite chemistry [33]. The measurement data are available in Zenodo [34].

The paper is organized as follows. In Section 2, we give a short overview of NODEs. Section 3 describes the modelling approach, presents the experimental basis, and shows how to normalize and initialize the learnable parameters and neural networks. Also, the simulation methodology as well as the training and test procedure are described. The results are shown and discussed in Section 4. In Section 5, we compare the GB model with results from our previous publication [32]. At the end of the paper, we summarize the results and give an outlook.

2. Background: Neural ordinary differential equations

NODEs are the continuous analogue of residual neural networks (ResNets) [35]. ResNets were introduced by [36]. Compared to simple feedforward networks, ResNets have additional short-cut connections. In a ResNet, the state transformation from layer t to layer $t+1$ can be described recursively [36]:

$$\boldsymbol{z}_{t+1} = \boldsymbol{z}_t + \boldsymbol{f}\left(\boldsymbol{z}_t, \boldsymbol{\theta}_t\right), \quad t = 0, \dots, T-1 \tag{1}$$

with the vector $\boldsymbol{z}_t \in \mathbb{R}^d$ of hidden states at layer t, the learned parameters $\boldsymbol{\theta}_t$ of layer t, and the learnable function $\boldsymbol{f} : \mathbb{R}^d \to \mathbb{R}^d$. The parameter vector $\boldsymbol{\theta}_t$ consists of the learned weights and biases. If the parameters are shared across the layers ($\boldsymbol{\theta}_t = \boldsymbol{\theta}$ for $t = 0, \dots, T-1$), a ResNet can be interpreted as the explicit Euler discretization of the initial value problem [35,37–39]

$$\frac{\mathrm{d}\boldsymbol{z}(t)}{\mathrm{d}t} = \boldsymbol{f}\left(\boldsymbol{z}(t), t, \boldsymbol{\theta}\right), \quad \boldsymbol{z}(0) = \boldsymbol{z}_0. \tag{2}$$

If we use a neural network to describe the derivative of the states with time directly, we end up with a NODE [35,40–42].

NODEs can be used for GB modelling [43,44]. Physically motivated differential equations and NODEs can be combined in one differential equation system or in a differential–algebraic system of equations and solved together [43,44]. In contrast to other neural networks for time-series prediction like ResNets and recurrent neural networks, NODEs can directly handle irregularly sampled data [35].

NODEs have been recently used for lithium-ion battery modelling. For example, Pepe et al. [45] used NODEs for predicting state of health, Ramasubramanian et al. [46] used NODEs for modelling SEI growth, and Brucker et al. [6] used NODEs for modelling the diffusion voltage.

3. Methodology

This section describes in detail the methodology summarized in Fig. 1(a). We first derive the equations for the Grey-Box ECM. We then describe the experimental basis. We further describe the initialization, normalization, simulation and optimization methodology. The section also includes an overview of the training and testing of the model.

3.1. Grey-box equivalent circuit model

3.1.1. Equivalent circuit model

The Grey-Box ECM derived in the following is shown in Fig. 1(b). It is modified from a combination of our previous work [6,32]. The ECM consists of an SOC-dependent voltage source, a series resistor and a GB diffusion element. The series resistance is approximated by two neural networks that form the BB model "BB". The diffusion element

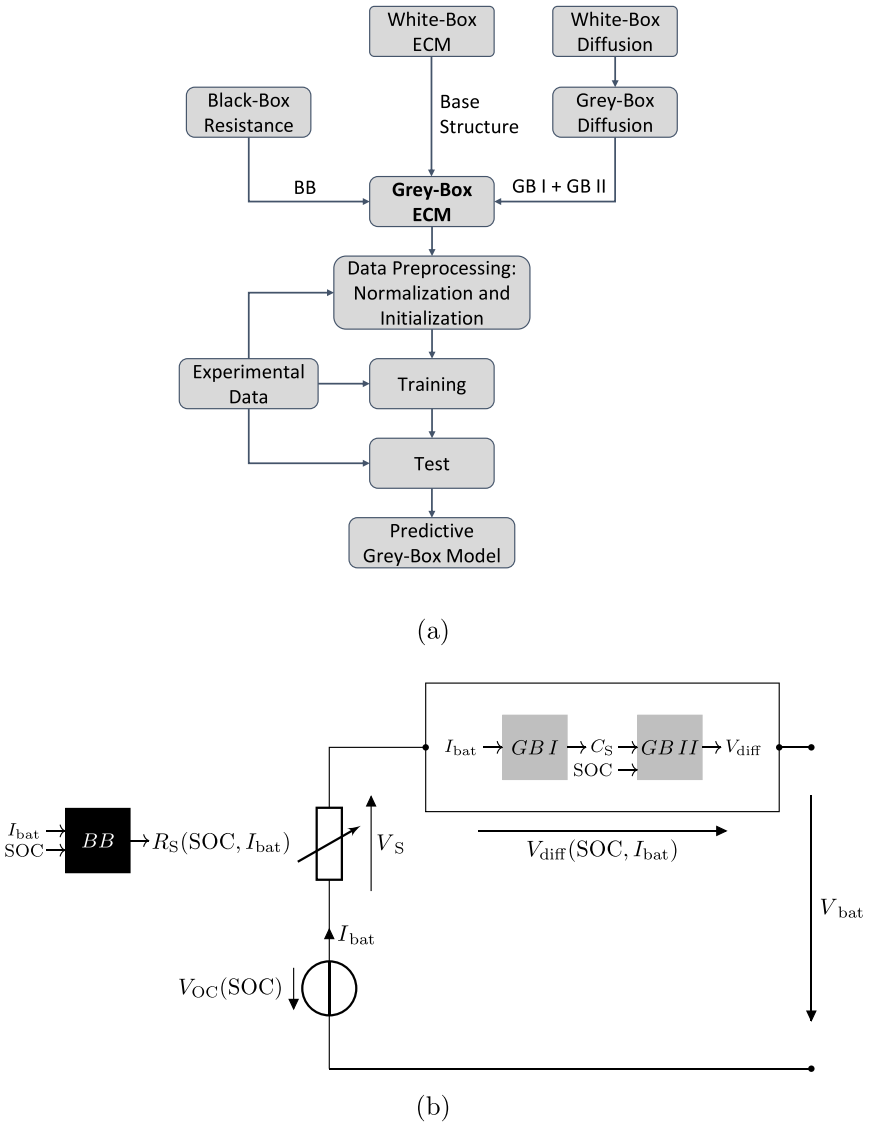

Fig. 1. (a) Overview of the modelling, training and testing approach used in the present work. (b) Grey-Box ECM of a lithium-ion battery consisting of an SOC-dependent voltage source V_{OC}, an SOC- and current-dependent series resistor R_S causing a voltage drop V_S, and a GB model for the diffusion voltage V_{diff} responsible for slow voltage dynamics. The series ohmic resistance is approximated by two neural networks. The diffusion voltage model was taken from Ref. [6] and consists of two individual parts: Firstly, the surface concentration C_S of a Fickian diffusion process is approximated (GB I). Secondly, the surface concentration in combination with the SOC of the battery is used to predict V_{diff} (GB II).

was developed based on a Warburg element, although it can describe dynamics other than pure Warburg-type behaviour [6]. It is represented by the two GB models "GB I" and "GB II".

The ECM can be described by the following system of equations:

$$\frac{\mathrm{dSOC}}{\mathrm{d}t} = -\frac{1}{C_{bat}} \cdot I_{bat} \tag{3a}$$

$$V_{bat} = V_{OC}(\mathrm{SOC}) - R_S(\mathrm{SOC}, I_{bat}) \cdot I_{bat} - V_{diff}(\mathrm{SOC}, I_{bat}) \tag{3b}$$

with the battery capacity C_{bat}, the ohmic resistance $R_S(\mathrm{SOC}, I_{bat})$ depending on SOC and battery current, the voltage drop V_{diff} across the diffusion element, and the SOC-dependent OCV $V_{OC}(\mathrm{SOC})$. The voltage drop V_S across the ohmic resistor R_S is given by Ohm's law. The battery voltage V_{bat} is the output of the dynamic system and the battery current I_{bat} is the external input. The current for discharging the battery is defined as positive and the current for charging the battery is defined as negative.

Eqs. (3) include unknown or imprecisely-known parameters and dependencies, in particular, $R_S(\mathrm{SOC}, I_{bat})$ and $V_{diff}(\mathrm{SOC}, I_{bat})$. For these, we introduce learnable parameters and neural networks, as shown in the following.

3.1.2. Slow voltage dynamics

In order to model the slow voltage dynamics, we integrate the models GB I and GB II introduced in Ref. [6] into the ECM shown in Fig. 1(b). These models are based on the finite-volume discretization of Fick's second law for diffusion in a cuboid particle with the length l. The model derivation and equations are summarized in Appendix A.1. The interested reader is referred to the original contribution [6] for more details.

The model equations for the diffusion element are given as [6]:

$$\frac{\partial \overline{C}_i}{\partial t} = \gamma_{i+1} - \gamma_i, \quad 0 \le i \le 4 \tag{4a}$$

$$\gamma_0 = 0 \tag{4b}$$

$$\gamma_i = |f\left(\frac{\overline{C}_i + \overline{C}_{i-1}}{2}, \theta_f\right)| \cdot \alpha_i \cdot \left(\overline{C}_i - \overline{C}_{i-1}\right), \quad 1 \le i \le 4 \tag{4c}$$

$$\gamma_5 = -\alpha_5 \cdot I_{\text{bat}} \tag{4d}$$

$$C_{\text{S}} = \frac{3\overline{C}_4 - \overline{C}_3}{2} \tag{4e}$$

$$V_{\text{diff}} = \omega_1 \cdot \left(\text{SOC} - C_{\text{S}}\right) \tag{4f}$$

with the learnable parameters α_i and ω_1 and the neural network f. The Eqs. (4a) to (4e) form the GB model "GB I" in Figs. 1(a) and 1(b). The Eq. (4f) represents "GB II". The battery current I_{bat} and SOC are the inputs to the model and the diffusion voltage V_{diff} is the output.

Based on the approach of Refs. [47–49] we use the following (partially) nondimensionalized quantities and functions to minimize the influence of rounding errors:

$$C = \frac{c - c_{\min}}{c_{\max} - c_{\min}};\ z = \frac{x}{\frac{l}{2}};\ \delta = \frac{j}{\frac{l}{2} \cdot \left(c_{\max} - c_{\min}\right)};\ D^*(C) = \frac{D(c)}{\left(\frac{l}{2}\right)^2} \tag{5}$$

where, c is the lithium concentration, $c_{\max}$ and $c_{\min}$ are the average concentrations when the battery is fully charged and empty, respectively, x is the length along the diffusion axis, j is the molar flux across the particle surface, and D is the diffusion coefficient. The scaling of the quantities also simplifies training (cf. Section 3.3).

As in Ref. [6], we use a feedforward network for f with one hidden layer, ten hidden neurons and ReLU activation. The nondimensionalized concentration is the network input and the partially nondimensionalized diffusion coefficient in s^{-1} is the output. The parameters α_i, $0 \le i \le 4$ represent dimensionless quantities. The parameter α_5, on the other hand, is given in $\text{A}^{-1}\,\text{s}^{-1}$. The unit of the parameter ω_1 is volts. We decided to use five discretization volumes for the diffusion domain, which previously resulted in good approximations for Fickian diffusion with nonlinear diffusion coefficient and long-timescale voltage dynamics, while the computational time was acceptable [6]. Note that the differential equation (4a) in combination with Eq. (4c) represents a NODE with incorporated prior knowledge.

In the present work, we integrate the GB model given by Eqs. (4) into the ECM given by Eqs. (3). Although the GB model was derived from the Fickian diffusion of lithium in one active material particle, we use it here to model the slow dynamics of a complete lithium-ion battery cell. Therefore, the average nondimensionalized concentration $\overline{C}$ represents the SOC of the battery.

3.1.3. Series ohmic resistance and open-circuit voltage

In Eq. (3b) the ohmic resistance R_{S} and its dependence on SOC and battery current are unknown. Since we wanted to take into account that the series resistance may have different values and characteristics during charging and discharging (as observed experimentally [33]), R_{S} is described by two neural networks which form the BB model in Fig. 1(b). The first neural network is selected for battery discharge or rest, and the second for battery charge.

Furthermore, an OCV curve (dependence of OCV on SOC) is required in Eq. (3b). The manufacturer usually provides only finite-rate charge/discharge curves. Therefore we used the $V_{\text{OC}}(\text{SOC})$ derived from quasi-OCV measurements in Ref. [33].

3.1.4. Model summary

Overall, using these assumptions, the Grey-Box ECM shown in Fig. 1(b) is given as:

$$\frac{\text{dSOC}}{\text{d}t} = -\frac{1}{\omega_0} \cdot I_{\text{bat}} \tag{6a}$$

$$\begin{aligned} V_{\text{bat}} &= V_{\text{OC}}(\text{SOC}) - R_{\text{S}}\left(\text{SOC}, I_{\text{bat}}\right) \cdot I_{\text{bat}} \\ &\quad - V_{\text{diff}}\left(\text{SOC}, I_{\text{bat}}\right) \end{aligned} \tag{6b}$$

$$R_{\text{S}}\left(\text{SOC}, I_{\text{bat}}\right) = \begin{cases} g\left(\text{SOC}, I_{\text{bat}}, \boldsymbol{\theta}_{\text{g}}\right), & I_{\text{bat}} < 0 \\ h\left(\text{SOC}, I_{\text{bat}}, \boldsymbol{\theta}_{\text{h}}\right), & I_{\text{bat}} \ge 0 \end{cases} \tag{6c}$$

$$V_{\text{diff}}\left(\text{SOC}, I_{\text{bat}}\right) = \omega_1 \cdot \left(\text{SOC} - C_{\text{S}}\right) \tag{6d}$$

$$\frac{\partial \overline{C}_i}{\partial t} = \gamma_{i+1} - \gamma_i, \quad 0 \le i \le 4 \tag{6e}$$

$$\gamma_0 = 0 \tag{6f}$$

$$\begin{aligned} \gamma_i &= \left| f\left(\frac{\overline{C}_i + \overline{C}_{i-1}}{2}, \boldsymbol{\theta}_{\text{f}}\right)\right| \cdot \alpha_i \cdot \left(\overline{C}_i - \overline{C}_{i-1}\right), \\ &\quad 1 \le i \le 4 \end{aligned} \tag{6g}$$

$$\gamma_5 = -\alpha_5 \cdot I_{\text{bat}} \tag{6h}$$

$$C_{\text{S}} = \frac{3 \cdot \overline{C}_4 - \overline{C}_3}{2} \tag{6i}$$

with the learnable parameters α_i, ω_0 and ω_1 and the feedforward networks f, g and h with their respective learnable parameters $\boldsymbol{\theta}_{\text{f}}$, $\boldsymbol{\theta}_{\text{g}}$ and $\boldsymbol{\theta}_{\text{h}}$. The parameter ω_0 represents the battery capacity while the other parameters represent the same quantities as before. The neural networks have one hidden layer each and use a ReLU activation function. Note that the neural network f has one input and ten hidden neurons, and the neural networks g and h have two inputs and 100 hidden neurons each. One of the inputs of the neural networks g and h is dimensionless, the other is given in amperes. The output of the neural networks g and h is a resistance value in ohms. When using a lower number of hidden neurons for g and h, the results deteriorated significantly. The SOC and current dependence could not be represented by the neural networks. Increasing the number of hidden neurons resulted in a higher computation time with similar simulation results [32]. Therefore, we decided to use 100 hidden neurons for g and h.

The "BB" model in Fig. 1(b) is given by Eq. (6c). The Eqs. (6e) to (6i) form the GB model "GB I" and Eq. (6d) represents "GB II" in Figs. 1(a) and 1(b). As before, the combination of Eqs. (6e) and (6g) results in a NODE with incorporated prior knowledge. Note that we have neither taken into account temperature dependencies nor ageing effects.

3.2. Experimental basis

We have applied the proposed Grey-Box ECM to a single large-format LFP-based lithium-ion battery cell. The prismatic cell from the Chinese manufacturer CALB (model CA180FI) has a nominal capacity of 180 A h and uses LFP at the positive electrode and graphite at the negative electrode.

We used the measurement data from Refs. [32,33] for training and testing the model. In particular, measurements for CCCV charging and discharging with different C-rates of 0.1 C, 0.28 C, and 1 C (corresponding to 18 A, 50 A, and 180 A respectively) during the constant current (CC) phase were used. The upper and lower cut-off voltages were 3.65 V and 2.5 V respectively, and a cut-off current of the constant voltage (CV) phase of $\text{C}/20$ was used. We also included one charge and one discharge curve with a pulsed current: During 50 A CC operation, the current was reduced every two SOC-percent to 25 A for 30 s. Additionally, a synthetic load profile representing a home storage battery was used for model testing. This synthetic load profile was taken from Ref. [50] and downscaled to the energy of the present cell. In all experiments, the ambient temperature was kept at $T_{\text{amb}} = 25\,^{\circ}\text{C}$. The experiments are described in more detail in the original paper [32]. To reduce the number of data points, we dropped measurement points that show no change compared to the previous data point. The measurement data (voltage and current versus time) are openly available in Zenodo [34]. It is difficult to apply neural networks, such as recurrent neural networks, to irregularly sampled data as given here due to the reduction of data points. The use of NODEs allows direct processing of irregularly sampled training data [35].

The measured battery current was used as the external input to the model. As suggested in Ref. [44], we linearly interpolated the measured current values to provide values at arbitrary times as required by the numerical solver.

3.3. Normalization and initialization

According to Ref. [51], the initialization and scaling of the parameters to be learned are crucial for good training. The authors of Ref. [51] recommend scaling the inputs of neural networks in a way that their average over the training set is close to zero (this is fulfilled for the battery current of a rechargeable battery since negative currents for charging and positive currents for discharging integrate to zero). In addition, the covariance of the input variables should be about the same.

We scaled the inputs of the neural networks to numerical values between approximately −1 and 1 which is consistent with the range of the SOC of 0 to 1. The neural network f takes a nondimensionalized average concentration as input. It is approximately in the range between 0 and 1. The neural networks g and h take the SOC and the battery current as inputs. The current values are scaled by the factor $1/180$ as the maximum current considered is 180 A. The average of the battery current over the training set is close to zero since the currents for charging are negative and the currents for discharging are positive.

We also normalized the output numerical values of the neural networks to an approximate range between 0 and 1. When scaling the learnable parameters we also considered the expected deviations from the chosen initial values.

The nominal capacity of the cell is given as $C_\mathrm{N} = 180\,\mathrm{A\,h}$ by the manufacturer. However, integrating the current over time for an entire charge or discharge cycle gives a charge throughput of $Q \approx 191.5\,\mathrm{A\,h}$ [32]. We scaled the learnable parameter by a factor of ten and initialized it with $\omega_0^* = 10^{-1} \cdot \omega_0 = 19.15\,\mathrm{A\,h}$. We used this scaling factor because we expected deviations from the initial value of up to several ampere-hours. As we used SI units in the model, we had to include an additional conversion factor in the corresponding differential equation.

Additionally, we had to estimate the series ohmic resistance in Eq. (3b), or rather its learnable representations in Eq. (6c). We therefore examined the measurement data from the pulse tests in more detail. From a representative pulse, the ohmic resistance could be estimated as $R_\mathrm{S} = |\Delta V/\Delta I| = 0.28\,\mathrm{m\Omega}$, which we use as initial value. Again, we introduced scaling factors to simplify the training process: $g\left(\mathrm{SOC}, I_\mathrm{bat}, \boldsymbol{\theta}_\mathrm{g}\right) = 10^{-3} \cdot g^*\left(\mathrm{SOC}, I_\mathrm{bat}/180, \boldsymbol{\theta}_{g^*}\right)$ and $h\left(\mathrm{SOC}, I_\mathrm{bat}, \boldsymbol{\theta}_\mathrm{h}\right) = 10^{-3} \cdot h^*\left(\mathrm{SOC}, I_\mathrm{bat}/180, \boldsymbol{\theta}_{\mathrm{h}^*}\right)$. We initialized the weights and biases of g^* and h^* from the uniform distribution $\mathcal{U}\left(-\sqrt{1/k}, \sqrt{1/k}\right)$, with $k \in \mathbb{N}$ the number of inputs to each layer (cf. Ref. [51]).

The learnable parameters concerning the voltage dynamics were estimated as before in Ref. [6], where the voltage drops across a Warburg element and an RC circuit were modelled. The scaled learnable parameters were set to $\omega_1^* = 0.1\,\mathrm{V}$, $\alpha_i^* = 1$ for $1 \le i \le 4$, and $\alpha_5^* = 0.5\,\mathrm{A^{-1}\,s^{-1}}$. The scaling factors were 10 for ω_1^*, 10^{-1} for $\alpha_i^*, 1 \le i \le 4$, and 10^{-5} for α_5^* (cf. Ref. [6]).

The final, scaled Grey-Box ECM is given by the following equation system:

$$\frac{\mathrm{dSOC}}{\mathrm{d}t} = -\frac{1}{10 \cdot \omega_0^* \cdot 3600\,\mathrm{s\,h^{-1}}} \cdot I_\mathrm{bat} \tag{7a}$$

$$V_\mathrm{bat} = V_\mathrm{OC}(\mathrm{SOC}) - R_\mathrm{S}\left(\mathrm{SOC}, I_\mathrm{bat}\right) \cdot I_\mathrm{bat} - V_\mathrm{diff}\left(\mathrm{SOC}, I_\mathrm{bat}\right) \tag{7b}$$

$$R_\mathrm{S}\left(\mathrm{SOC}, I_\mathrm{bat}\right) = \begin{cases} 10^{-3} \cdot g^*\left(\mathrm{SOC}, I_\mathrm{bat}/180, \boldsymbol{\theta}_{g^*}\right), & I_\mathrm{bat} < 0 \\ 10^{-3} \cdot h^*\left(\mathrm{SOC}, I_\mathrm{bat}/180, \boldsymbol{\theta}_{\mathrm{h}^*}\right), & I_\mathrm{bat} \ge 0 \end{cases} \tag{7c}$$

$$V_\mathrm{diff}\left(\mathrm{SOC}, I_\mathrm{bat}\right) = 10 \cdot \omega_1^* \cdot \left(\mathrm{SOC} - C_\mathrm{S}\right) \tag{7d}$$

$$\frac{\partial \overline{C}_i}{\partial t} = \gamma_{i+1} - \gamma_i, \quad 0 \le i \le 4 \tag{7e}$$

$$\gamma_0 = 0 \tag{7f}$$

$$\gamma_i = 0.1 \cdot \left| f^*\left(\frac{\overline{C}_i + \overline{C}_{i-1}}{2}, \boldsymbol{\theta}_{\mathrm{f}^*}\right)\right| \cdot \alpha_i^* \cdot \left(\overline{C}_i - \overline{C}_{i-1}\right), \quad 1 \le i \le 4 \tag{7g}$$

$$\gamma_5 = -10^{-5} \cdot \alpha_5^* \cdot I_\mathrm{bat} \tag{7h}$$

$$C_\mathrm{S} = \frac{3 \cdot \overline{C}_4 - \overline{C}_3}{2} \tag{7i}$$

with the scaled parameters ω_0^*, ω_1^* and $\alpha_i^*, 1 \le i \le 5$ and the feedforward networks f^*, g^* and h^*. Since the scaling factors are dimensionless, the scaled parameters have the same units as the unscaled ones. The neural networks correspond in size and configuration to the neural networks f, g and h in the Eqs. (6).

Again, the combination of Eqs. (7e) and (7g) represents a NODE with incorporated prior knowledge.

3.4. Simulation and training methodology

The model was implemented in Python (version 3.7.6). We used the open-source machine learning framework PyTorch (version 1.11.0) [52] which provides two main features: Tensor computing and automatic differentiation for neural networks. We furthermore used the torchdiffeq library (version 0.2.3) [53] to solve differential equations and NODEs and for the backpropagation of the training loss. The differential equations were solved with the Dopri5 method with an absolute tolerance of 10^{-9} and a relative tolerance of 10^{-7} unless otherwise stated. The OCV curve was implemented as a look-up table and evaluated by linear interpolation. Here we used the linear interpolation from xitorch (version 0.3.0) [54] to allow for backpropagation.

For training, different loss functions were used, as will be defined further below. The training loss was backpropagated through the differential equations and NODEs with the standard method from torchdiffeq which applies the chain rule. Finally, we used an Adam optimizer for loss minimization.

In order to simulate electrochemical impedance spectra of the final model, we used the rapid computational approach from Bessler [55]. We set the initial concentrations in the discretization elements and the initial SOC to 0.6. Starting with zero current, we simulated a current step of $\Delta I_\mathrm{bat} = 1.8\,\mathrm{A}$ during $10^{-5}\,\mathrm{s}$. We considered a simulation time of $7.2 \cdot 10^4\,\mathrm{s}$. We calculated the impedance according to the algorithm in Ref. [55] for a frequency band between $10^{-5}\,\mathrm{Hz}$ and 10 Hz. A proper choice of solvers and tolerance turned out to be important for the impedance simulations. When using the Dopri5 method with an absolute tolerance of 10^{-9} and a relative tolerance of 10^{-7} we got a very noisy impedance spectrum. The results improved significantly with lower absolute and relative tolerances of 10^{-20}.

3.5. Training

The model has a large number of unknown parameters that need to be identified by training: The 7 learnable parameters ω_0^*, ω_1^* and $\alpha_i^*, 1 \le i \le 5$ and the parameters $\boldsymbol{\theta}_{\mathrm{f}^*}$, $\boldsymbol{\theta}_{\mathrm{g}^*}$ and $\boldsymbol{\theta}_{\mathrm{h}^*}$ in the three neural networks f^*, g^* and h^*. The neural network f^* has an input neuron, a hidden layer of ten neurons, and an output neuron. The weights and biases add up to 31 parameters in $\boldsymbol{\theta}_{\mathrm{f}^*}$. The neural networks g^* and h^* have two input neurons, a hidden layer of 100 neurons, and one output neuron each. $\boldsymbol{\theta}_{g^*}$ and $\boldsymbol{\theta}_{\mathrm{h}^*}$ consist of 401 parameters each. In total, the GB model has $7 + 31 + 401 + 401 = 840$ parameters.

Due to the small amount of training data available, we split the training into several parts: First, we trained the neural networks g^* and h^* for all values of SOC and an absolute battery current $|I_\mathrm{bat}| = 25\,\mathrm{A}$ and $|I_\mathrm{bat}| = 50\,\mathrm{A}$. We then trained the parameters associated with the diffusion voltage. The next step was to optimize the pre-trained parameters. We then focused on the pulsed current data, in particular, to optimize the parameters that influence the dynamics of the battery. Finally, we took into account all the training data. The interested reader is referred to Appendix A.2 for a detailed description of the training procedure.

In total, we ran 500 training epochs with stochastic gradient descent. During each training epoch, the considered time series of the training data set were given to the model in random order. The learnable parameters were saved when the total training loss decreased during an epoch.

As there were few data available, we did not split off a validation data set.

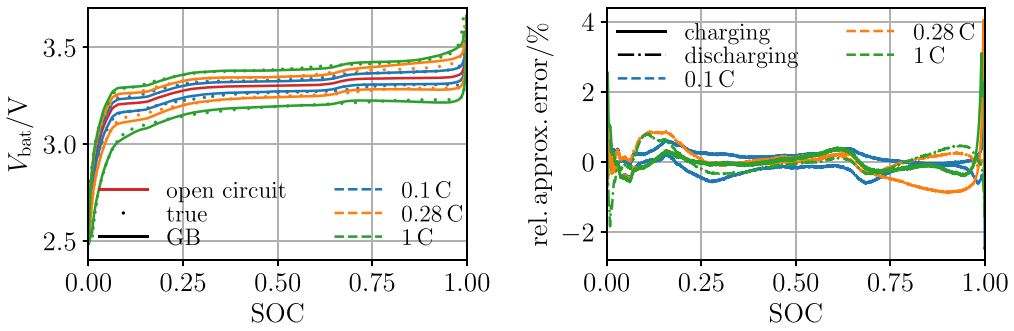

Fig. 2. Trained GB model, as presented in Fig. 1(b), in comparison to experimental CCCV data of an LFP-based lithium-ion battery; left: charge and discharge curves for different C-rates at $T_{amb} = 25\,°C$. The lower branches represent discharge (time progresses from right to left), while the upper branches represent charge (time progresses from left to right); right: relative voltage approximation error.

Table 1
Results for the scaled learnable parameters after finishing the training procedure, as well as the mean squared error (MSE) between the true and learned battery voltage for charging with a pulsed current.

$\alpha_1^*/-$	$\alpha_2^*/-$	$\alpha_3^*/-$	$\alpha_4^*/-$	$\alpha_5^*/(A^{-1}\,s^{-1})$	$\omega_0^*/A\,h$	ω_1^*/V	$MSE/10^{-4}\ V^2$
1.1538	1.1100	0.9281	0.8373	0.7252	19.1249	0.1362	4.2226

3.6. Test

We tested the final GB model against the synthetic load profile (cf. Section 3.2). We had to provide initial values for the SOC and the nondimensionalized average concentrations $\overline{C}_i$. We proceeded in the same way as for training: We derived the initial SOC from the battery voltage and initialized the average concentrations with the same value.

4. Results

In this section, we first compare the training results with the measured data. We then analyse the model behaviour and evaluate the output of the neural networks and the learnable parameters after training. We also apply the model to the test data.

4.1. Comparison of model against training data

In total, eight experimental time series of the LFP cell were used to train the GB model. Six of these time series represent charging and discharging with CCCV protocol at different C-rates, and the remaining two time series represent charging and discharging with pulsed currents.

Fig. 2 shows the training results for CCCV charging and discharging. Here we have chosen a voltage versus SOC plot, which allows a better comparison of different C-rates than a voltage versus time plot. The SOC was calculated according to Eq. (7a). The left panel shows measured and learned battery voltage. The right panel shows the relative voltage approximation error. The simulation results are in good agreement with the experiments over the complete SOC range and for all investigated C-rates. The relative approximation error is less than 1% for a wide range of SOC. Only for very low and very high SOC values, the absolute value of the relative approximation error reaches up to around 4%. As the OCV curve (shown in red in the left panel of Fig. 2) is very steep at low and high SOC, higher approximation errors can be expected in these regions.

LFP-based lithium-ion batteries exhibit a hysteresis behaviour of the open-circuit voltage between charge and discharge [56]. This is visible in Fig. 2 (left panel) as a significant voltage difference between charge and discharge branches even at the lowest C-rate. It is worth noting that the simulation is able to reproduce this behaviour correctly, even though the model does not explicitly take hysteresis into account.

Long-timescale battery dynamics are the focus of this study. Therefore, we next focus on the dynamic parts. Fig. 3 compares the trained model with experimental data of pulsed current charging. In contrast to the previous figure, we have chosen a temporal representation. The top panels show the entire time series, the middle panels zoom in on two current pulses at intermediate SOC, and the bottom panels focus on the final rest phase. The left panels show the battery current, the centre panels the battery voltage, and the right panels the individual voltage contributions of the equivalent circuit elements. Table 1 gives the mean squared error (MSE) between the true and the approximated battery voltage for charging with a pulsed current.

As shown in the upper (overview) panels, the approximated battery voltage is in good agreement with the measured voltage for most of the charging process. Towards the end of charging, when the SOC is high, there are larger deviations between the model approximation and the measured data. Similar results can be found for discharging (results not shown): The voltage cannot be reproduced for low values of SOC at the end of the discharging process. This is in agreement with the high approximation errors at low and high values of SOC for CCCV charging and discharging. The absolute value of V_S increases towards the end of charging where the battery is (nearly) fully charged, both for a current load of $-25\,A$ and $-50\,A$. The absolute value of the diffusion voltage V_{diff} tends to decrease as the charging time progresses.

As shown in the middle panels of Fig. 3, the voltage response following the current pulses at intermediate SOC is reproduced by the model in a qualitatively correct way. The deviation between the measurement data and the model prediction is low. However, it increases as the duration of a constant current load increases. This is particularly true towards the end of the period shown.

As shown in the lower panels, the model cannot reproduce the true battery voltage for high values of SOC and rest phases. The absolute value of the voltage drop V_S across the series resistor decreases with the current. During the rest phase, it is zero. The absolute value of the diffusion voltage V_{diff} also decreases with decreasing current. However, there is still a contribution at the beginning of the rest phase. A comparison of the voltages in the rest phase shows that the relaxation in the model is too fast. Additionally, the absolute value of the approximated diffusion voltage is too low at the beginning of the rest phase. There is a huge deviation between the final measured and approximated voltages. The approximated voltage drops across the series resistor and the diffusion element are (close to) zero at the end of the time series. The approximated battery voltage is determined by the OCV. This suggests that the predicted SOC is inaccurate. The results are similar for discharging when the battery is (nearly) empty.

The GB model can, all in all, reproduce the training data well for medium SOC values. For low and high SOC values the voltage cannot be predicted correctly. The use of more training data, especially in regions with high and low SOC values, could lead to an improvement of the modelling results. In addition, a stronger weighting of training errors in these regions could be beneficial.

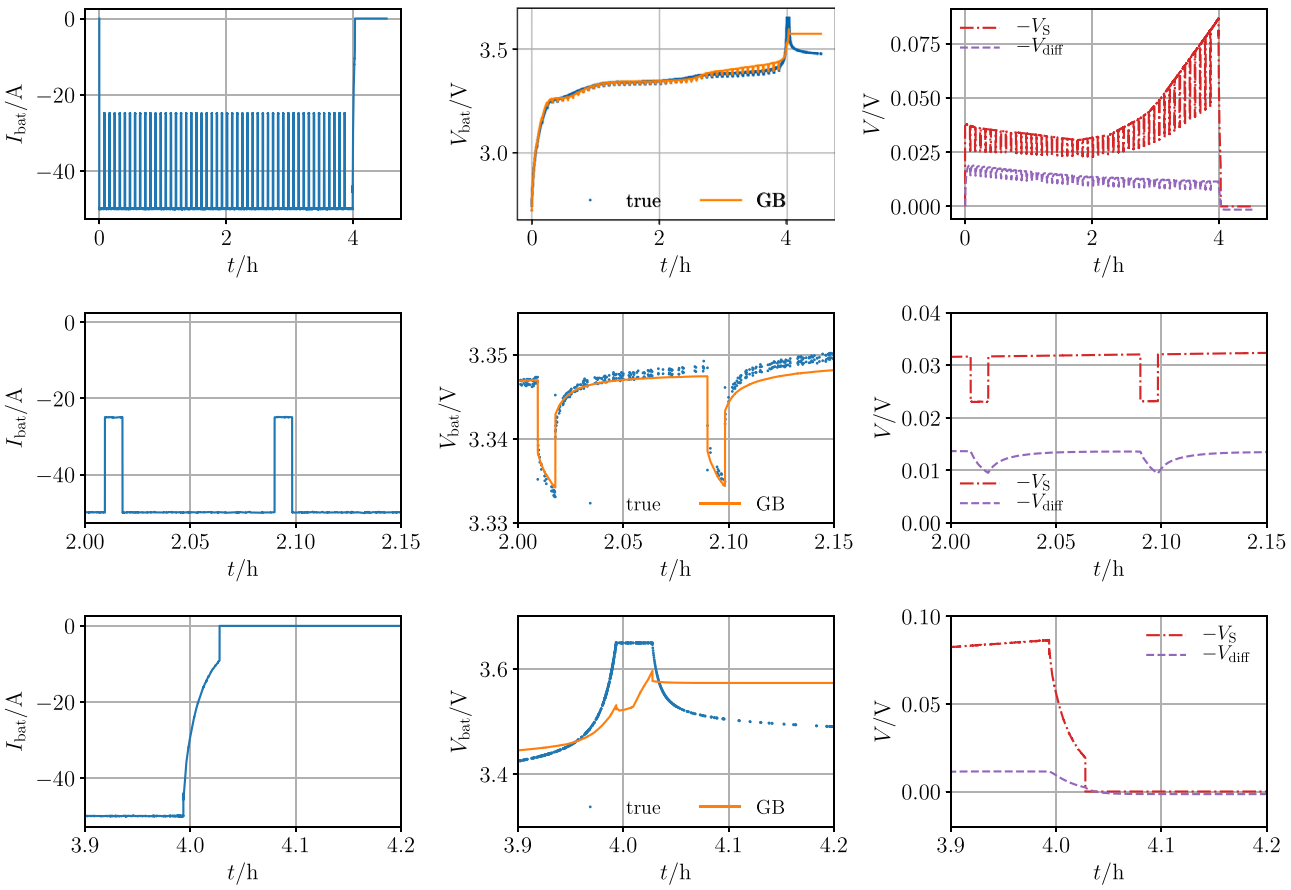

Fig. 3. Trained GB model compared to experimental data for charging with a pulsed current. The upper panels show the complete time series, the middle panels zoom in on two current pulses in the middle of the time series, the lower panels zoom in on the final rest phase; left: battery current; middle: battery voltage; right: individual voltage contributions of the ohmic resistor and the diffusion element.

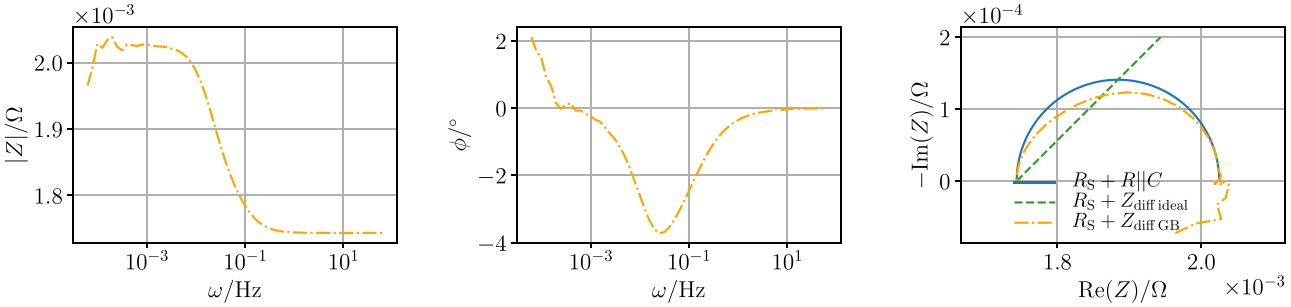

Fig. 4. Simulated electrochemical impedance spectrum of the serial connection of the ohmic resistor and the diffusion element of the trained GB model at 50% SOC; left: amplitude response, middle: phase response, right: Nyquist plot in comparison to an ideal Warburg element and an ideal resistor-capacitor circuit.

4.2. Model behaviour

We further investigated the GB modelling results. Fig. 4 shows simulated electrochemical impedance spectra at a medium SOC for the series connection of the ohmic resistor R_S and the diffusion element Z_{diff} of the trained GB model. The left panel shows the amplitude response, the middle panel shows the phase response and the right panel shows the resulting Nyquist plot. The ohmic resistor causes an offset V_S on the x axis of the Nyquist plot. For comparison, we also show the Nyquist plot of a pure Warburg element and an RC circuit, using the same offset. The series ohmic resistance R_S was determined through evaluation of the neural network h^* at the chosen initial SOC and for a current of $I_{bat} = 1.8$ A. The ohmic resistance of the fictitious RC circuit was derived from the maximum voltage $V_{diff\,max}$ following the current step. The Nyquist plot of the GB model represents neither a semicircle nor a straight line at high frequencies. The behaviour is inbetween these two limiting cases. The battery does not exhibit ideal Warburg-type or RC-type behaviour.

The diffusion voltage element used in our GB model is based on a Fickian diffusion model. It is therefore interesting to take a closer look at the concentration profiles in the diffusion domain. Fig. 5 shows the predicted SOC and concentrations for pulsed charging (same simulation run as shown in Fig. 3). The GB model concentrations at the surface, and the average concentration in the middle discretization element (indicated with 2 in the legend) and in the innermost discretization element (indicated with 0 in the legend) are shown. According to the definition of the nondimensionalized concentration, the SOC is equal to the average concentration of the whole particle. Therefore, the SOC should always lie between the concentration in the innermost volume element and the surface concentration. This is true for the CC phase.

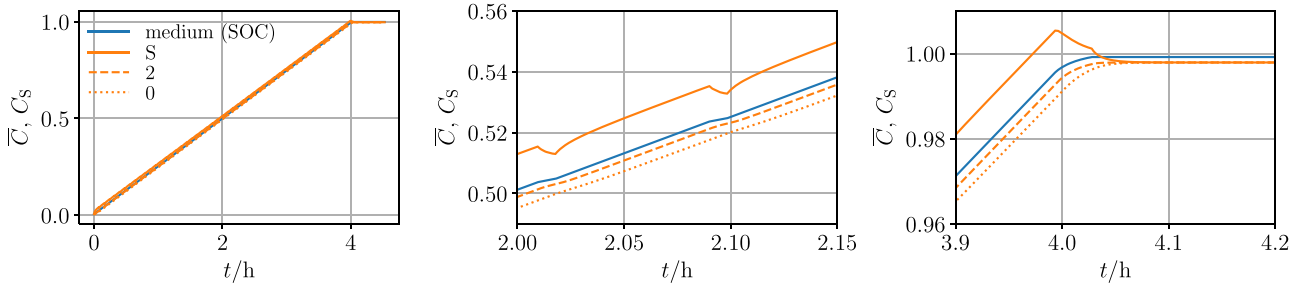

Fig. 5. Simulated concentration dynamics during charging with a pulsed current (same simulation run as in Fig. 3); left: concentration profile in comparison to the SOC over the whole time series; middle: two current pulses in the middle of the time series; right: the last segment. The legend indicates the position within the diffusion length, where S is the surface, 2 is the middle discretization element and 0 is the innermost element.

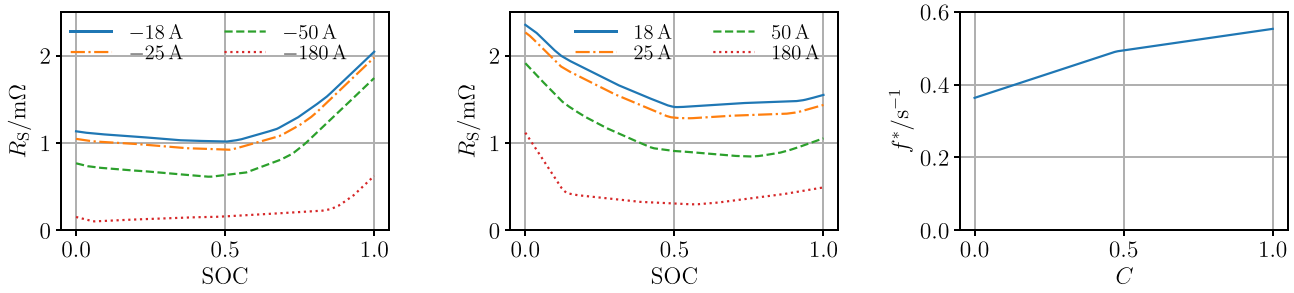

Fig. 6. Output of the trained neural networks; left: R_S as a function of SOC for different battery currents for charging; middle: R_S as a function of SOC for different battery currents for discharging; right: f^*, representing the diffusion coefficient, as a function of concentration.

However, during the rest phase, when the concentrations approach each other the predicted SOC is slightly higher than the predicted concentrations. The approximated SOC and/or concentrations are therefore slightly inaccurate.

4.3. Output of trained neural networks and parameters

We used the two neural networks g^* and h^* to approximate the dependence of the ohmic resistance R_S on current and SOC. Fig. 6 shows the training results for R_S for different battery currents over the complete SOC range. The left panel shows the results for charging ($I_{bat} < 0$ A) evaluated with g^*. The middle panel shows the results for discharging (and rest $I_{bat} \geq 0$ A) evaluated with h^*. The ohmic resistance is in the range of up to several milliohms. It increases as the absolute battery current decreases, both during charging and discharging, and reaches higher values at low and high SOC, compared to intermediate SOC. There is an asymmetry between charging and discharging: During charging, the ohmic resistance reaches its highest values at high SOC. During discharging, this is the case at low SOC. This behaviour is known for lithium-ion batteries with LFP electrode [33].

The right panel of Fig. 6 shows the output of the scaled neural network f^* after training. This neural network represents the concentration-dependent diffusion coefficient. It shows a slight sectional linear dependence on the concentration. A physical interpretation of this behaviour is difficult; it represents the macroscopic cell behaviour as identified by the model training.

The scaled learnable parameters α_i^*, ω_0^* and ω_1^* are given in Table 1. The parameters α_1^* to α_4^* represent the lengths of the individual discretization volumes. The values decrease slightly with increasing i, which means that the discretization volumes become larger towards the surface. Again, a physical interpretation is difficult. Note that in our previous publication [6], the parameters α_i^* increased with increasing i for an ideal Warburg impedance model, and decreased significantly with increasing i for an ideal RC circuit model. For the Warburg impedance model, the concentration change following a current step was largest at the particle surface, with a clear propagation into the inner discretization volumes [6]. For the RC circuit model, however, the concentrations in the inner discretization volumes were only slightly changed [6]. In the present model, the concentrations propagate into the particle (cf. Fig. 6). Therefore, the dynamic behaviour of the battery is neither of RC circuit type nor of Warburg type.

4.4. Comparison of model against test data

We tested the final GB model against test data not included in the training. The test data set represents a synthetic load profile of a home-storage battery. The results are shown in Fig. 7. The upper panels cover the entire time series, while the lower panels focus on a dynamic part in the middle. In the overview (upper panels), the simulated voltage shows good agreement with the experimental data. The largest errors occur in the regions of high measured battery voltage. It is worth noting that the synthetic load profile covers a long measurement time with $t \approx 52.8$ h. The longest training time series covers only $t \approx 11.6$ h.

The lower panels show a dynamic part of the data in the middle of the time series. The model shows clear deviations from experiments, both in the absolute voltage levels and in the voltage dynamics. The approximation error is particularly high for phases of low-current charge (negative currents at around 31.9 h, 32.0 h and 32.2 h). If we take a closer look at the individual contributions of the series resistor and the diffusion element, it is clear that it is mainly the resistor that causes the approximation error. It should be noted that we did not include data with low absolute currents at medium SOC values in the training.

5. Discussion: Model comparison

In this section, we compare the Grey-Box ECM introduced here to our previous work on a simpler ECM [32]. In particular, in our previous work, the dynamics of the battery were modelled with a simple RC circuit. We will therefore refer to this model as RC-circuit model. The charge-transfer resistance was considered to depend on the battery current and the SOC, and was modelled with two neural networks, one for charging and one for discharging. We used the same measurement data for training and testing of the model as in the present study. The

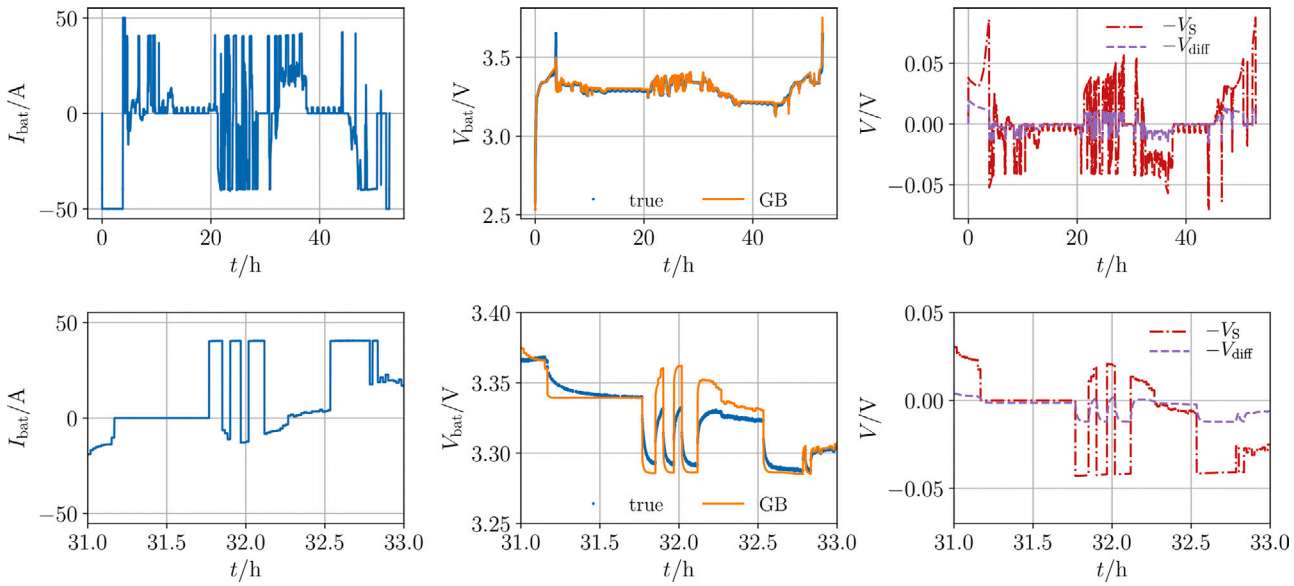

Fig. 7. Test results in comparison to experimental data representing a synthetic load profile of a home-storage battery system. The upper panels show the full time series, while the lower panels zoom in on the dynamic part in the middle of the time series; left: battery current; middle: battery voltage; right: individual voltage contributions of the ohmic resistor and the diffusion element.

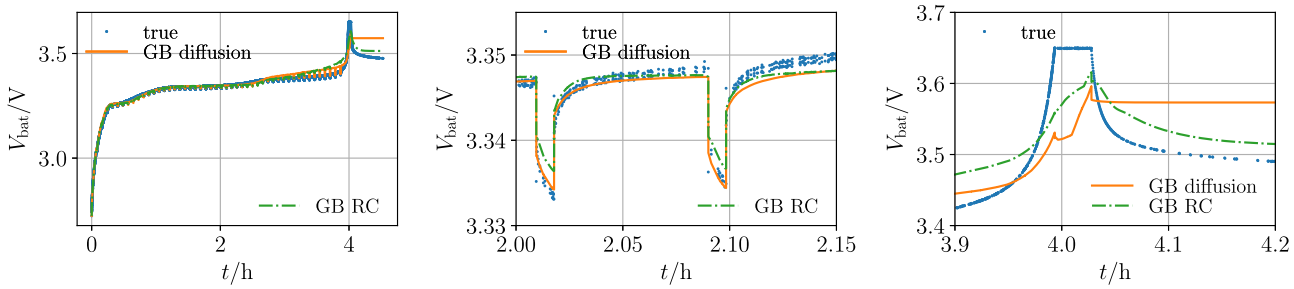

Fig. 8. Comparison of results from two different GB models, a simple one with RC circuit (taken from our previous work [32]), and a more complex one with diffusion element (present work); left: voltage response over the whole time series; middle: two current pulses in the middle of the time series; right: the final CV phase and rest.

previous results from Ref. [32] are compared to results from this work in Fig. 8 for pulsed charging.

Overall, both models can describe the battery voltage in good agreement with the measured data. The overall view in the left panel of Fig. 8 shows that the RC-circuit model deviates more from the measured voltage towards the end of charging. During pulses (middle panel), the RC-circuit model also performs worse than the new GB model including diffusion. Here, the ohmic voltage drop is underestimated by the RC-circuit model. In addition, when using the RC-circuit model, the characteristics of the time behaviour also differ from the experiment. The new diffusion model can capture the voltage dynamics more accurately. The CV and the rest phase (right panel) cannot be represented correctly by either the RC-circuit model or the diffusion model.

In summary, the comparison shows that the more complex model structure of the diffusion model leads to an increase in prediction accuracy compared to the RC-circuit model.

A direct comparison of our Grey-Box ECM against other models from previous research (e.g., [57,58]) is not possible within the scope of the present work, because different battery cells and different measurement data were used. A comparison between the different modelling methodologies, after applying them to the same experimental data, must be left to future studies.

6. Summary and conclusions

In this article we have presented the development, training, and application of a GB model for lithium-ion batteries including slow voltage dynamics. The model is based on an ECM with voltage source, series resistor, and diffusion element. The series resistance is parameterized as a function of SOC and current using neural networks. The diffusion element is based on a discretized form of Fickian diffusion, parameterized using a neural network and learnable parameters [6]. The model is flexible to represent not only Warburg-type behaviour, but also other dynamics like RC behaviour. Mathematically, the model is described by a differential–algebraic equation system combining algebraic, ordinary, and neural differential equations. This framework has a number of advantages: It combines concepts of both physics-based theory (WB model) and artificial intelligence (BB model) into a combined framework (GB model). This allows a smaller amount of training data, compared to BB approaches. The model can describe the battery dynamics in the time domain. It avoids difficult-to-solve fractional time-domain differential equations resulting from pure Fickian diffusion [59]. Because NODEs and differential equations are solved together, irregularly-sampled input data can be easily handled, allowing to reduce computational time. Other neural networks for time series prediction, such as recurrent neural networks, can only describe regularly-sampled input data.

We have shown that the model can successfully describe the experimental voltage behaviour of a large-format LFP-based lithium-ion cell. In particular, the well-known charge–discharge hysteresis and asymmetric overpotentials of LFP-based cells were successfully reproduced. A particular focus of the study was the long-timescale (10 s scale) battery dynamics that occur during load changes. The diffusion element was able to reproduce the experimentally-observed voltage dynamics during pulse tests.

Despite the overall successful demonstration of the model, several details in the battery behaviour are not reproduced correctly, compared to the experiments. Towards very high and very low SOC, the model is unable to correctly capture the voltage and its dynamics of the training data. Also, dynamic voltage behaviour in the test data during current steps is captured only qualitatively, not quantitatively. At the present point, it is unclear if these discrepancies are inherent to the model structure itself, or due to insufficient training. The training database was rather small: only six time series covering CCCV charging and discharging with different C-rates and two time series with pulsed charging and discharging were used for training.

In future work, it would be interesting to include more extensive training data from pulse tests with different current steps and rest periods. Also, the use of real-world operation data for training will be worthwhile studying. The applicability of the model framework to other battery chemistries (e.g., NMC-based lithium-ion cells) is yet to be shown. It should also be noted that we included neither temperature dependencies nor ageing effects in the model.

In conclusion, we have shown that the use of NODEs with incorporated prior knowledge can be a powerful methodology for GB modelling of lithium-ion batteries with a particular focus on battery dynamics.

CRediT authorship contribution statement

Jennifer Brucker: Writing – review & editing, Writing – original draft, Validation, Software, Methodology, Investigation, Formal analysis, Conceptualization. **Rainer Gasper:** Supervision, Project administration, Funding acquisition, Conceptualization. **Wolfgang G. Bessler:** Writing – review & editing, Supervision, Conceptualization.

Declaration of competing interest

The authors declare that they have no known competing financial interests or personal relationships that could have appeared to influence the work reported in this paper.

Data availability

The measurement data is available in Zenodo [34]. Code will be made available on request.

Declaration of Generative AI and AI-assisted technologies in the writing process

During the preparation of this work the author(s) used DeepL Write in order to shorten and/or rewrite some paragraphs to improve readability. After using this tool/service, the author(s) reviewed and edited the content as needed and take(s) full responsibility for the content of the publication.

Acknowledgements

J.B. and R.G. acknowledge funding from the Carl Zeiss Foundation, Germany. J.B. is an associated member of the Research Training Group GRK 2218 SiMET—Simulation of mechano-electro-thermal processes in lithium-ion batteries, project number: 281041241. She thanks the German Research Foundation (DFG) for the cooperative support. We acknowledge support by the Open Access Publication Fund of the Offenburg University of Applied Sciences, Germany.

Appendix

A.1. Grey-box model for the diffusion voltage

In this section we give a brief summary of the derivation of the "GB I" and "GB II" models introduced in our previous publication [6]. Additionally, we highlight the main results from Ref. [6].

Diffusion in the active material particles of the battery electrodes is described by Fick's laws. Fick's second law describes the spatiotemporal change of concentrations as follows [60]:

$$\frac{\partial c}{\partial t} = \nabla (D \nabla c) \tag{A.1}$$

with the concentration c, the diffusion coefficient D, and the Nabla operator ∇. In Ref. [6] we assumed that the active material particles are cuboid and diffusion only takes place in one direction. The electrochemical reaction takes place only at the surface of the particle. A (de)intercalation process with a constant diffusion current through the particle surface leads to the following initial and boundary conditions [47–49,61]:

$$c = c_{\text{init}}, \quad 0 \le x \le \frac{l}{2}, t = 0 \tag{A.2a}$$

$$\frac{\partial c}{\partial x} = 0, \quad x = 0, t \ge 0 \tag{A.2b}$$

$$-D\frac{\partial c}{\partial x} = j_{\text{influx}}, \quad x = \frac{l}{2}, t \ge 0 \tag{A.2c}$$

with the initial concentration c_{init}, and the molar flux across the particle surface j_{influx}. The particle centre is at $x = 0$, and the particle surface is at $x = l/2$. [6]

We used the (partially) nondimensionalized quantities and functions according to Eqs. (5):

$$C = \frac{c - c_{\min}}{c_{\max} - c_{\min}}; \; z = \frac{x}{\frac{l}{2}}; \; \delta = \frac{j}{\frac{l}{2} \cdot (c_{\max} - c_{\min})}; \; D^*(C) = \frac{D(c)}{\left(\frac{l}{2}\right)^2}$$

where $c_{\max}$ and $c_{\min}$ are the medium concentrations when the battery is completely full or empty, respectively. According to this definition, the average concentration $\overline{C}$ of the considered particle represents the SOC of the electrode or the whole battery cell. [6]

We applied the finite volume discretization to Fick's second law for diffusion in a cuboid particle [6]:

$$\frac{\partial \overline{C}_i}{\partial t} = \frac{\delta_{i+1} - \delta_i}{z_{i+1} - z_i}, \quad 0 \le i \le N-1 \tag{A.3a}$$

$$\delta_i = 2 \cdot \frac{D^*\left(\frac{\overline{C}_i + \overline{C}_{i-1}}{2}\right) \cdot \left(\overline{C}_i - \overline{C}_{i-1}\right)}{z_{i+1} - z_{i-1}}, \quad 1 \le i \le N-1 \tag{A.3b}$$

$$\delta_0 = 0 \tag{A.3c}$$

$$\delta_N = \frac{j_{\text{influx}}}{\frac{l}{2} \cdot (c_{\max} - c_{\min})} \tag{A.3d}$$

$$\overline{C}_{i,0} = C_{\text{init}}, \quad 0 \le i \le N-1. \tag{A.3e}$$

The authors of [62] recommend a linear extrapolation to approximate the surface concentration C_S:

$$C_S = \frac{3\overline{C}_{N-1} - \overline{C}_{N-2}}{2}. \tag{A.4}$$

Under the assumption of small perturbations around the equilibrium a connection between concentration and potential can be derived based on the Nernst equation [63,64]:

$$V_{\text{diff}} = \frac{R_g T}{F}\left(\ln \frac{c_{\text{v act}}}{c_{\text{v eq}}} - \ln \frac{c_{\text{Li act}}}{c_{\text{Lieq}}}\right) \tag{A.5}$$

with the universal gas constant R_g, the temperature T, the Faraday constant F, and the concentrations of intercalated lithium $c_{\text{Li act}}$ and c_{Lieq}, and the concentrations of vacancies $c_{\text{v act}}$ and $c_{\text{v eq}}$. Here, the subscripts

act and eq indicate the actual and the equilibrium concentration at the considered point of operation. [6]

In Ref. [6] we reformulated Eq. (A.5) and applied it to the solid state diffusion of lithium in the active material particles. We neglected the influence of vacancies [6]:

$$V_{\mathrm{diff}} = -a \ln \frac{c_{\mathrm{S}}}{\bar{c}} \tag{A.6}$$

with a proportionality factor a, the surface concentration c_{S} of lithium and the mean lithium concentration $\bar{c}$ in the particle. We applied the logarithmic laws $\ln \frac{c_{\mathrm{S}}}{\bar{c}} = \ln c_{\mathrm{S}} - \ln \bar{c}$ and used the nondimensionalized quantities C_{S} and $\overline{C}$ instead of c_{S} and $\bar{c}$. We linearized the logarithmic terms and used $\overline{C} = \mathrm{SOC}$. Finally, we ended up with the following simplified expression:

$$V_{\mathrm{diff}} = \omega_1 \cdot \left(\mathrm{SOC} - C_{\mathrm{S}}\right) \tag{A.7}$$

with the learnable parameter ω_1. Herein, the SOC of the battery can be determined by current integration:

$$\frac{\mathrm{dSOC}}{\mathrm{d}t} = -\frac{1}{C_{\mathrm{bat}}} \cdot I_{\mathrm{bat}} \tag{A.8}$$

with the battery capacity C_{bat}. [6]

We used the Eqs. (A.3), (A.4), (A.7), and (A.8) as a starting point for GB modelling of diffusion processes. We replaced unknown or imprecisely known parameters and dependencies with learnable parameters and neural networks. Overall, we derived the following GB model according to Eqs. (4) and (A.8) in Ref. [6]:

$$\begin{aligned}
\frac{\partial \overline{C}_i}{\partial t} &= \gamma_{i+1} - \gamma_i, \quad 0 \le i \le 4 \\
\gamma_0 &= 0 \\
\gamma_i &= |f\left(\frac{\overline{C}_i + \overline{C}_{i-1}}{2}, \theta_{\mathrm{f}}\right)| \cdot \alpha_i \cdot \left(\overline{C}_i - \overline{C}_{i-1}\right), \quad 1 \le i \le 4 \\
\gamma_5 &= -\alpha_5 \cdot I_{\mathrm{bat}} \\
C_{\mathrm{S}} &= \frac{3\overline{C}_4 - \overline{C}_3}{2} \\
\frac{\mathrm{dSOC}}{\mathrm{d}t} &= -\frac{1}{C_{\mathrm{bat}}} \cdot I_{\mathrm{bat}} \\
V_{\mathrm{diff}} &= \omega_1 \cdot \left(\mathrm{SOC} - C_{\mathrm{S}}\right)
\end{aligned}$$

with the learnable parameters α_i and ω_1 and the neural network f. The GB model takes the battery current as input to approximate the diffusion voltage V_{diff}. [6]

In Ref. [6] the GB modelling approach was used to approximate the concentration dynamics of Fickian diffusion (without the equations for the SOC and V_{diff}), voltage dynamics of a Warburg element, and voltage dynamics of an RC circuit. The model was trained and tested with simulation data. After appropriate training, the GB model was able to approximate the different dynamics with good accuracy. The GB model should therefore be capable of modelling experimental data including non-ideal Warburg- or RC-type behaviour. [6]

The interested reader is referred to Ref. [6] for a more detailed description of the GB modelling approach and its usage for modelling different long timescale dynamics.

A.2. Training procedure

The training of the GB model is briefly described in Section 3.5. Here we give a more detailed insight into the different training steps.

In total, we ran 500 training epochs with stochastic gradient descent. During the first 49 training epochs we only considered Eq. (7c) to approximate the parameters θ_{g^*} and θ_{h^*}. We required $R_{\mathrm{S\,true}} = 0.28\ \mathrm{m\Omega}$ for all values of SOC at an absolute current of $|I_{\mathrm{bat}}| = 25\ \mathrm{A}$ and $|I_{\mathrm{bat}}| = 50\ \mathrm{A}$. We only trained the parameters θ_{g^*} and θ_{h^*} and used the MSE of the demanded and the approximated series ohmic resistance to define the loss function L as

$$L = 1000 \cdot \mathrm{MSE}\left(1000 \cdot R_{\mathrm{S\,GB}}/\Omega, 1000 \cdot R_{\mathrm{S\,true}}/\Omega\right). \tag{A.9}$$

An Adam optimizer with a decaying learning rate between $l = 10^{-2}$ and $l = 10^{-3}$ minimized the loss.

After completing the first 49 training epochs, we considered the entire GB model for the remainder of the training. Absolute current values less than 0.25 A were set to 0 A. To evaluate the function we had to know the initial values of the SOC and the concentrations $\overline{C}_0$ to $\overline{C}_4$. We determined the initial SOC equal to the average concentrations at the corresponding times by inverting the $V_{\mathrm{OC}}(\mathrm{SOC})$ curve and evaluating the resulting function with the measured battery voltage. We used the approximated and measured battery voltage to define the training loss. For charging and discharging with pulsed currents, we weighted the loss more heavily for absolute current values of about 25 A. We also penalized negative values for the ohmic resistance and negative outputs of the neural network f^*. For the latter, we calculated the output of f^* for input values in the range between −1 and 2 in steps of 0.1. We chose this wide range of values because due to our definition of the nondimensionalized concentration, it is also possible to get negative values or values greater than 1. Overall, the loss function was defined as follows:

$$L = 100 \cdot \mathrm{MSE}\left(100 \cdot V_{\mathrm{bat\,GB}}/\mathrm{V}, 100 \cdot V_{\mathrm{bat\,true}}/\mathrm{V}\right) \tag{A.10a}$$

$$\textbf{if } 22\ \mathrm{A} < |I_{\mathrm{bat}}| < 28\ \mathrm{A}: \quad L = L + \mathrm{MSE}\left(100 \cdot V_{\mathrm{bat\,GB}}/\mathrm{V}, 100 \cdot V_{\mathrm{bat\,true}}/\mathrm{V}\right) \tag{A.10b}$$

$$\textbf{if } R_{\mathrm{S\,GB}} < 0\ \Omega: \quad L = L - 1000000 \cdot R_{\mathrm{S\,GB}}/\Omega \tag{A.10c}$$

$$\textbf{for } x = -1 \textbf{ to } 2 \textbf{ step } 0.1 \quad \textbf{if } f^*(x) < 0\,\mathrm{s}^{-1}: \quad L = L - 10000 \cdot f^*(x)/\mathrm{s}^{-1} \tag{A.10d}$$

We performed backpropagation through the differential equations and NODEs using the standard odeint method from torchdiffeq and used PyTorch's automatic differentiation for the algebraic equations. An Adam optimizer with a decaying learning rate between $l = 10^{-2}$ and $l = 10^{-4}$ minimized the loss.

During the training epochs 50 to 74 we used the CCCV training data. From epoch 50 to epoch 59, we only allowed an adjustment of the parameters θ_{f^*} and α_i^*. Afterwards, we additionally freed the parameters θ_{g^*} and θ_{h^*}. As there is a rest period at the end of each time series in the training data set, the battery should be approximately in equilibrium at the end. Therefore the concentrations $\overline{C}_0$ to $\overline{C}_4$ should be equal to the SOC of the battery. We added a term to the basic loss function to penalize the respective deviation of the predicted final SOC, the final concentration in the innermost discretization volume as well as the surface concentration from the SOC calculated from the battery voltage measured at the end of the time series.

From training epoch 75 to epoch 149, the focus was on the dynamic behaviour of the battery. Therefore, we only considered the training data from charging and discharging with pulsed currents. In addition to the aforementioned parameters, we allowed the adaptation of ω_1^*. During the epochs 75 to 99 we only considered the first 6000 data points of each time series. We then increased the number of data points to 10^4. Starting from epoch 125, we used the entire data series for training and released the parameter ω_0^*. When considering the whole time series, we took the additional penalization term into account.

During epochs 150 to 199, we continued with the training as before. However, we used all available training data.

Starting from epoch 200, we only optimized the parameters θ_{g^*} and θ_{h^*} during the next 250 epochs to further improve the approximation of the ohmic resistance.

Finally, we released all parameters during the last 51 training epochs to refine the GB model. Again, we took the additional penalization term into account. However, we only considered this penalization term for charging with pulsed currents and for charging according to the CCCV protocol with a current of −18 A or −50 A during the CC phase. These time series were chosen because of the long rest period after the current excitation.

References

[1] M.S. Ziegler, J.E. Trancik, Re-examining rates of lithium-ion battery technology improvement and cost decline, Energy Environ. Sci. 14 (4) (2021) 1635–1651, http://dx.doi.org/10.1039/D0EE02681F, URL https://pubs.rsc.org/en/content/articlelanding/2021/ee/d0ee02681f.

[2] U. Krewer, F. Röder, E. Harinath, R.D. Braatz, B. Bedürftig, R. Findeisen, Review—dynamic models of li-ion batteries for diagnosis and operation: A review and perspective, J. Electrochem. Soc. 165 (16) (2018) A3656–A3673, http://dx.doi.org/10.1149/2.1061814jes.

[3] M.S. Hosen, R. Gopalakrishnan, T. Kalogiannis, J. Jaguemont, J. van Mierlo, M. Berecibar, Impact of relaxation time on electrochemical impedance spectroscopy characterization of the most common lithium battery technologies—experimental study and chemistry-neutral modeling, World Electr. Veh. J. 12 (2) (2021) 77, http://dx.doi.org/10.3390/wevj12020077, URL https://www.mdpi.com/2032-6653/12/2/77.

[4] L. Pei, R. Lu, C. Zhu, Relaxation model of the open–circuit voltage for state–of–charge estimation in lithium–ion batteries, IET Electr. Syst. Transp. 3 (4) (2013) 112–117, http://dx.doi.org/10.1049/iet-est.2013.0020.

[5] L. Pei, T. Wang, R. Lu, C. Zhu, Development of a voltage relaxation model for rapid open-circuit voltage prediction in lithium-ion batteries, J. Power Sources 253 (2014) 412–418, http://dx.doi.org/10.1016/j.jpowsour.2013.12.083, URL https://www.sciencedirect.com/science/article/pii/S0378775313020624.

[6] J. Brucker, W.G. Bessler, R. Gasper, A grey-box model with neural ordinary differential equations for the slow voltage dynamics of lithium-ion batteries: Model development and training, J. Electrochem. Soc. 170 (12) (2023) 120537, http://dx.doi.org/10.1149/1945-7111/ad14cd.

[7] A.A. Franco, M.L. Doublet, W.G. Bessler (Eds.), Physical Multiscale Modeling and Numerical Simulation of Electrochemical Devices for Energy Conversion and Storage: From Theory To Engineering To Practice, first ed., Green Energy and Technology, Springer, London, 2016, http://dx.doi.org/10.1007/978-1-4471-5677-2.

[8] A. Seaman, T.-S. Dao, J. McPhee, A survey of mathematics-based equivalent-circuit and electrochemical battery models for hybrid and electric vehicle simulation, J. Power Sources 256 (2014) 410–423, http://dx.doi.org/10.1016/j.jpowsour.2014.01.057.

[9] S. Wang, P. Takyi-Aninakwa, S. Jin, C. Yu, C. Fernandez, D.-I. Stroe, An improved feedforward-long short-term memory modeling method for the whole-life-cycle state of charge prediction of lithium-ion batteries considering current–voltage-temperature variation, Energy 254 (2022) 124224, http://dx.doi.org/10.1016/j.energy.2022.124224, URL https://www.sciencedirect.com/science/article/pii/S0360544222011276.

[10] S. Wang, Y. Fan, S. Jin, P. Takyi-Aninakwa, C. Fernandez, Improved anti-noise adaptive long short-term memory neural network modeling for the robust remaining useful life prediction of lithium-ion batteries, Reliab. Eng. Syst. Saf. 230 (2023) 108920, http://dx.doi.org/10.1016/j.ress.2022.108920, URL https://www.sciencedirect.com/science/article/pii/S095183202200535X.

[11] S. Estrada-Flores, I. Merts, B. de Ketelaere, J. Lammertyn, Development and validation of grey-box models for refrigeration applications: A review of key concepts, Int. J. Refrig. 29 (6) (2006) 931–946, http://dx.doi.org/10.1016/j.ijrefrig.2006.03.018.

[12] Y. Oussar, G. Dreyfus, How to be a gray box: dynamic semi-physical modeling, Neural Netw. 14 (9) (2001) 1161–1172, http://dx.doi.org/10.1016/S0893-6080(01)00096-X.

[13] B. Duarte, P.M. Saraiva, C.C. Pantelides, Combined mechanistic and empirical modelling, Int. J. Chem. React. Eng. 2 (1) (2004) http://dx.doi.org/10.2202/1542-6580.1128.

[14] F. Hamilton, A.L. Lloyd, K.B. Flores, Hybrid modeling and prediction of dynamical systems, PLoS Comput. Biol. 13 (7) (2017) e1005655, http://dx.doi.org/10.1371/journal.pcbi.1005655.

[15] H. He, R. Xiong, J. Fan, Evaluation of lithium-ion battery equivalent circuit models for state of charge estimation by an experimental approach, Energies 4 (4) (2011) 582–598, http://dx.doi.org/10.3390/en4040582.

[16] Y. Wang, H. Fang, L. Zhou, T. Wada, Revisiting the state-of-charge estimation for lithium-ion batteries: A methodical investigation of the extended kalman filter approach, IEEE Control Syst. 37 (4) (2017) 73–96, http://dx.doi.org/10.1109/MCS.2017.2696761.

[17] J.A. Braun, R. Behmann, D. Schmider, W.G. Bessler, State of charge and state of health diagnosis of batteries with voltage-controlled models, J. Power Sources 544 (2022) 231828, http://dx.doi.org/10.1016/j.jpowsour.2022.231828, URL https://www.sciencedirect.com/science/article/pii/S0378775322008175.

[18] C. Fleischer, W. Waag, H.-M. Heyn, D.U. Sauer, On-line adaptive battery impedance parameter and state estimation considering physical principles in reduced order equivalent circuit battery models: Part 1. requirements, critical review of methods and modeling, J. Power Sources 260 (2014) 276–291, http://dx.doi.org/10.1016/j.jpowsour.2014.01.129.

[19] M. Chen, G.A. Rincón-Mora, Accurate electrical battery model capable of predicting runtime and I–V performance, IEEE Trans. Energy Convers. 21 (2) (2006) 504–511, http://dx.doi.org/10.1109/TEC.2006.874229.

[20] D. Haifeng, W. Xuezhe, S. Zechang, A new SOH prediction concept for the power lithium-ion battery used on HEVs, in: 2009 IEEE Vehicle Power and Propulsion Conference, 2009, pp. 1649–1653, http://dx.doi.org/10.1109/VPPC.2009.5289654.

[21] Y. Hu, S. Yurkovich, Y. Guezennec, B.J. Yurkovich, A technique for dynamic battery model identification in automotive applications using linear parameter varying structures, Control Eng. Pract. 17 (10) (2009) 1190–1201, http://dx.doi.org/10.1016/j.conengprac.2009.05.002.

[22] S. Tong, M.P. Klein, J.W. Park, On-line optimization of battery open circuit voltage for improved state-of-charge and state-of-health estimation, J. Power Sources 293 (2015) 416–428, http://dx.doi.org/10.1016/j.jpowsour.2015.03.157.

[23] M.E. Fouda, A.S. Elwakil, A.G. Radwan, A. Allagui, Power and energy analysis of fractional-order electrical energy storage devices, Energy 111 (2016) 785–792, http://dx.doi.org/10.1016/j.energy.2016.05.104.

[24] Q.-K. Wang, Y.-J. He, J.-N. Shen, Z.-F. Ma, G.-B. Zhong, A unified modeling framework for lithium-ion batteries: An artificial neural network based thermal coupled equivalent circuit model approach, Energy 138 (2017) 118–132, http://dx.doi.org/10.1016/j.energy.2017.07.035, URL https://www.sciencedirect.com/science/article/pii/S0360544217312100.

[25] M. Luzi, M. Paschero, A. Rizzi, E. Maiorino, F.M. Frattale Mascioli, A novel neural networks ensemble approach for modeling electrochemical cells, IEEE Trans. Neural Netw. Learn. Syst. 30 (2) (2019) 343–354, http://dx.doi.org/10.1109/TNNLS.2018.2827307.

[26] M. Luzi, F.M. Frattale Mascioli, M. Paschero, A. Rizzi, A white-box equivalent neural network circuit model for SoC estimation of electrochemical cells, IEEE Trans. Neural Netw. Learn. Syst. 31 (2) (2020) 371–382, http://dx.doi.org/10.1109/TNNLS.2019.2901062.

[27] S. Leonori, L. Baldini, A. Rizzi, F.M. Frattale Mascioli, A physically inspired equivalent neural network circuit model for SoC estimation of electrochemical cells, Energies 14 (21) (2021) 7386, http://dx.doi.org/10.3390/en14217386, URL https://www.mdpi.com/1996-1073/14/21/7386.

[28] G. Fan, K. Pan, M. Canova, J. Marcicki, X.G. Yang, Modeling of li-ion cells for fast simulation of high C-rate and low temperature operations, J. Electrochem. Soc. 163 (5) (2016) A666–A676, http://dx.doi.org/10.1149/2.0761605jes, URL https://iopscience.iop.org/article/10.1149/2.0761605jes.

[29] J. Marcicki, M. Canova, A.T. Conlisk, G. Rizzoni, Design and parametrization analysis of a reduced-order electrochemical model of graphite/$LiFePO_4$ cells for SOC/SOH estimation, J. Power Sources 237 (2013) 310–324, http://dx.doi.org/10.1016/j.jpowsour.2012.12.120, URL https://www.sciencedirect.com/science/article/pii/S0378775313000694.

[30] W. Luo, C. Lyu, L. Wang, L. Zhang, An approximate solution for electrolyte concentration distribution in physics-based lithium-ion cell models, Microelectron. Reliab. 53 (6) (2013) 797–804, http://dx.doi.org/10.1016/j.microrel.2012.11.002, URL https://www.sciencedirect.com/science/article/pii/S0026271412005100.

[31] X. Li, G. Fan, K. Pan, G. Wei, C. Zhu, G. Rizzoni, M. Canova, A physics-based fractional order model and state of energy estimation for lithium ion batteries. Part I: Model development and observability analysis, J. Power Sources 367 (2017) 187–201, http://dx.doi.org/10.1016/j.jpowsour.2017.09.049, URL https://www.sciencedirect.com/science/article/pii/S0378775317312570.

[32] J. Brucker, R. Behmann, W.G. Bessler, R. Gasper, Neural ordinary differential equations for grey-box modelling of lithium-ion batteries on the basis of an equivalent circuit model, Energies 15 (7) (2022) 2661, http://dx.doi.org/10.3390/en15072661.

[33] M.C. Yagci, R. Behmann, V. Daubert, J.A. Braun, D. Velten, W.G. Bessler, Electrical and structural characterization of large–format lithium iron phosphate cells used in home–storage systems, Energy Technol. 9 (6) (2021) 202000911, http://dx.doi.org/10.1002/ente.202000911.

[34] J. Brucker, R. Behmann, W.G. Bessler, R. Gasper, Code and measurement data - neural ordinary differential equations for grey-box modelling of lithium-ion batteries on the basis of an equivalent circuit model, Code Meas. Data (2022) http://dx.doi.org/10.5281/zenodo.6323623, URL https://zenodo.org/record/6323623.

[35] R.T.Q. Chen, Y. Rubanova, J. Bettencourt, D. Duvenaud, Neural ordinary differential equations, 2018, arXiv:1806.07366.

[36] K. He, X. Zhang, S. Ren, J. Sun, Deep residual learning for image recognition, in: 29th IEEE Conference on Computer Vision and Pattern Recognition, IEEE, Piscataway, NJ, 2016, pp. 770–778.

[37] E. Haber, L. Ruthotto, Stable architectures for deep neural networks, Inverse Problems 34 (1) (2018) 014004, http://dx.doi.org/10.1088/1361-6420/aa9a90.

[38] L. Ruthotto, E. Haber, Deep neural networks motivated by partial differential equations, J. Math. Imaging Vision 62 (2020) 352–364.

[39] E. Haber, L. Ruthotto, E. Holtham, S.-H. Jun, Learning across scales – multiscale methods for convolution neural networks, in: Proceedings of the AAAI Conference on Artificial Intelligence, Vol. 32, AAAI Press, Palo Alto, California USA, 2018, pp. 3142–3148, http://dx.doi.org/10.1609/aaai.v32i1.11680.

[40] E. Dupont, A. Doucet, Y.W. Teh, Augmented neural ODEs, in: Advances in Neural Information Processing Systems, Vol. 32, Curran Associates, Inc., Red Hook, NY, USA, 2019, pp. 3140–3150.

[41] T. Zhang, Z. Yao, A. Gholami, K. Keutzer, J. Gonzalez, G. Biros, M.W. Mahoney, ANODEV2: A coupled neural ODE evolution framework, 2019, arXiv:1906.04596.

[42] A. Gholami, K. Keutzer, G. Biros, ANODE: Unconditionally accurate memory-efficient gradients for neural ODEs, in: Proceedings of the Twenty-Eighth International Joint Conference on Artificial Intelligence, International Joint Conferences on Artificial Intelligence, 2019, pp. 730–736.

[43] C. Rackauckas, Y. Ma, J. Martensen, C. Warner, K. Zubov, R. Supekar, D. Skinner, A. Ramadhan, A. Edelman, Universal differential equations for scientific machine learning, 2020, http://dx.doi.org/10.48550/arXiv.2001.04385, arXiv:2001.04385.

[44] J. Brucker, W.G. Bessler, R. Gasper, Grey-box modelling of lithium-ion batteries using neural ordinary differential equations, Energy Inf. 4 (Suppl 3) (2021) 15, http://dx.doi.org/10.1186/s42162-021-00170-8, URL https://energyinformatics.springeropen.com/articles/10.1186/s42162-021-00170-8.

[45] S. Pepe, J. Liu, E. Quattrocchi, F. Ciucci, Neural ordinary differential equations and recurrent neural networks for predicting the state of health of batteries, J. Energy Storage 50 (2022) 104209, http://dx.doi.org/10.1016/j.est.2022.104209, URL https://www.sciencedirect.com/science/article/pii/S2352152X22002407.

[46] S. Ramasubramanian, F. Schomburg, F. Röder, Modelling of solid electrolyte interphase growth using neural ordinary differential equations, Electrochim. Acta 473 (2024) 143479, http://dx.doi.org/10.1016/j.electacta.2023.143479, URL https://www.sciencedirect.com/science/article/pii/S0013468623016511.

[47] V.R. Subramanian, J.A. Ritter, R.E. White, Approximate solutions for galvanostatic discharge of spherical particles: I. Constant diffusion coefficient, J. Electrochem. Soc. 148 (11) (2001) E444–E449, http://dx.doi.org/10.1149/1.1409397.

[48] M. Guo, R.E. White, An approximate solution for solid-phase diffusion in a spherical particle in physics-based li-ion cell models, J. Power Sources 198 (2012) 322–328, http://dx.doi.org/10.1016/j.jpowsour.2011.08.096, URL https://www.sciencedirect.com/science/article/pii/S0378775311016430.

[49] S. Liu, An analytical solution to Li/Li^+ insertion into a porous electrode, Solid State Ion. 177 (1–2) (2006) 53–58, http://dx.doi.org/10.1016/j.ssi.2005.09.053.

[50] B. Weißhar, W.G. Bessler, Model-based lifetime prediction of an LFP/graphite lithium-ion battery in a stationary photovoltaic battery system, J. Energy Storage 14 (2017) 179–191, http://dx.doi.org/10.1016/j.est.2017.10.002.

[51] Y. LeCun, L. Bottou, G.B. Orr, K.-R. Müller, Efficient backprop, in: G.B. Orr, K.-R. Müller (Eds.), Neural Networks: Tricks of the Trade, Springer Berlin Heidelberg, Berlin, Heidelberg, 1998, pp. 9–50.

[52] A. Paszke, S. Gross, F. Massa, A. Lerer, J. Bradbury, G. Chanan, T. Killeen, Z. Lin, N. Gimelshein, L. Antiga, A. Desmaison, A. Kopf, E. Yang, Z. DeVito, M. Raison, A. Tejani, S. Chilamkurthy, B. Steiner, L. Fang, J. Bai, S. Chintala, Pytorch: An imperative style, high-performance deep learning library, in: Advances in Neural Information Processing Systems, Vol. 32, Curran Associates, Inc., Red Hook, NY, USA, 2019, pp. 8024–8035.

[53] R.T.Q. Chen, Torchdiffeq, 2021, URL https://github.com/rtqichen/torchdiffeq.

[54] M.F. Kasim, Xitorch, 2020, URL https://github.com/xitorch/xitorch.

[55] W.G. Bessler, Rapid impedance modeling via potential step and current relaxation simulations, J. Electrochem. Soc. 154 (11) (2007) B1186–B1191, http://dx.doi.org/10.1149/1.2772092, URL https://www.researchgate.net/publication/225000354_Rapid_Impedance_Modeling_via_Potential_Step_and_Current_Relaxation_Simulations.

[56] W. Dreyer, J. Jamnik, C. Guhlke, R. Huth, J. Moskon, M. Gaberscek, The thermodynamic origin of hysteresis in insertion batteries, Nature Mater. 9 (5) (2010) 448–453, http://dx.doi.org/10.1038/nmat2730.

[57] D. Zhu, J.J. Campbell, G. Cho, Battery voltage prediction using neural networks, in: IEEE Transportation Electrification Conference & Expo, ITEC, IEEE, 2021, pp. 807–812, http://dx.doi.org/10.1109/ITEC51675.2021.9490081.

[58] A.G. Li, K. Mayilvahanan, A.C. West, M. Preindl, Discrete-time modeling of li-ion batteries with electrochemical overpotentials including diffusion, J. Power Sources 500 (2021) 229991, http://dx.doi.org/10.1016/j.jpowsour.2021.229991, URL https://www.sciencedirect.com/science/article/pii/S037877532100519X.

[59] M. Hu, Y. Li, S. Li, C. Fu, D. Qin, Z. Li, Lithium-ion battery modeling and parameter identification based on fractional theory, Energy 165 (2018) 153–163, http://dx.doi.org/10.1016/j.energy.2018.09.101, URL https://www.sciencedirect.com/science/article/pii/S0360544218318656.

[60] R.B. Bird, W.E. Stewart, E.N. Lightfoot, Transport Phenomena, Revised second ed., John Wiley & Sons Inc, New York and Chichester and Weinheim and Brisbane and Singapore and Toronto, 2007.

[61] T.F. Fuller, M. Doyle, J. Newman, Simulation and optimization of the dual lithium ion insertion cell, J. Electrochem. Soc. 141 (1) (1994) 1–10, http://dx.doi.org/10.1149/1.2054684.

[62] Y. Zeng, P. Albertus, R. Klein, N. Chaturvedi, A. Kojic, M.Z. Bazant, J. Christensen, Efficient conservative numerical schemes for 1D nonlinear spherical diffusion equations with applications in battery modeling, J. Electrochem. Soc. 160 (9) (2013) A1565–A1571, http://dx.doi.org/10.1149/2.102309jes, URL https://iopscience.iop.org/article/10.1149/2.102309jes/meta.

[63] E. Barsoukov, J.R. Macdonald, Impedance Spectroscopy: Theory, Experiment, and Applications, second ed., John Wiley & Sons, Inc., Hoboken, New Jersey, 2005, http://dx.doi.org/10.1002/0471716243.

[64] M. Schönleber, C. Uhlmann, P. Braun, A. Weber, E. Ivers-Tiffée, A consistent derivation of the impedance of a lithium-ion battery electrode and its dependency on the state-of-charge, Electrochim. Acta 243 (2017) 250–259, http://dx.doi.org/10.1016/j.electacta.2017.05.009, URL https://www.sciencedirect.com/science/article/pii/S0013468617309805.